Autofocus system for microscope

Qingxiang Li
Lifen Bai
Shifu Xue
Luyun Chen
Tsinghua University
Department of Precision Instruments and Mechanology
Beijing 100084
E-mail: bailf@ntl.pim.tsinghua.edu.cn

Abstract. A technique is developed for microscope autofocusing, which is called the eccentric light beam approach with high resolution, wide focusing range, and compact construction. The principle is described. The theoretical formula of the eccentric light beam approach deduced can be applied not only to an object lens whose objective plane is just at the focal plane, but also to an object lens whose objective plane is not at the focal plane. The experimental setup uses a semiconductor laser device as the light source. The laser beam that enters into the microscope is eccentric with the main light axis. A defocused signal is acquired by a symmetrical silicon photocell for the change of the reflected light position caused by differential amplification and processed by a microprocessor. Then the electric signal is power-amplified and drives a dc motor, which moves a fine working platform to an automatic focus of the microscope. The result of the experiments shows a ± 0.1-μm precision of autofocusing for a range of ± 500-μm defocusing. The system has high reliability and can meet the requirements of various accurate micro measurement systems.
[DOI: 10.1117/1.1473639]

Subject terms: autofocus; microscope; eccentric-light-beam approach.

Paper 200487 received Dec. 8, 2000; revised manuscript received Nov. 2, 2001; accepted for publication Dec. 11, 2001.

1. Introduction

Focusing is one of the most important techniques in optical instruments. It appeared in 1970s with the development of the video disk, and after that more and more researchers worked on it. There were many patents and papers on autofocusing in recent years, most of which apply to camera systems.

The earliest autofocusing device was a pneumatic focus servo device that utilized the pneumatic principle in a closed-loop feedback system and had a precision less than $\pm 50\ \mu$m with a ± 200-μm focus range.[1] In the skew beam method, use is made of an auxiliary narrow beam that passes the objective off axis, then the returning beam hits one of two detectors. The difference photosignal is a linear measure of the defocus around the image plane in focus. This method has a very large acquisition range; for example, it senses over tens of tracks in the optical readout of a video disk. Another method, the Foucault knife-edge test, in its original version is not very practical because of the sever tolerance on the lateral knife-edge position. A modification of the Foucault knife-edge method adds a prism with a large apex angle to diminish the severe tolerance on the lateral knife-edge position in its original version. The beam that reflects back from the disk through the objective is incident on a prism with a large apex angle, where the converging beam is refracted into two beams, each of which shows the characteristic Foucault intensity distribution as a function of the defocusing of the beam with respect to the apex of the prism. The acquisition range can be[2] 1 mm. In the astigmatic method, a cylindrical lens is inserted in the beam between the beamsplitter and the final image. The light spot is a circle when the surface is in focus and becomes an ellipse when it is out of focus. Depending on whether the surface is positioned too low or too high, the long axis of the ellipse is in one direction or at 90 deg. An acquisition range of 40 μm is typical.[3,4] All these autofocus methods present advantages and disadvantages, and each method has its different application.

In the late decade, autofocusing techniques were used in many fields, such as an multilayered optical disk for high-density storage, microscopic image analysis of defect areas in optical disks, multiple blurred objects image restoration, and surveillance camera system.[5–8]

In microscope systems, the depth of field is small, the tolerance is even smaller, and the operating distance is also short, so an important requirement of the precision is proposed. With the recent development in science and technology, the requirement of high precision and automation are proposed. Besides the image quality of a microscope system itself, the focusing precision often influences the measurement precision to a great extent. Especially when the measurement is repeated at different times, the difference of focusing will cause large errors. Today, most of the autofocusing systems in micrometry use processed images as an indirect measure for defocus, but the repetition precision of this method depends on the image quality. A direct autofocusing system is sound solution to this problem on account of it being more compact and robust than the former one. A confocal scanning optical microscope uses a direct focus-detection technique to characterize a surface topography whose accuracy is within 10 nm with a measurement range of 0.5 μm; it is suitable for the high accuracy and small range measurement.[9] In this paper, a wide-range direct autofocus system is developed according to he principle of the eccentric light beam method.

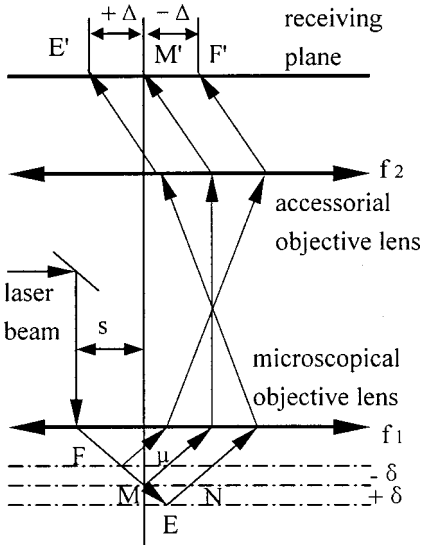

Fig. 1 Principle of the eccentric light beam method.

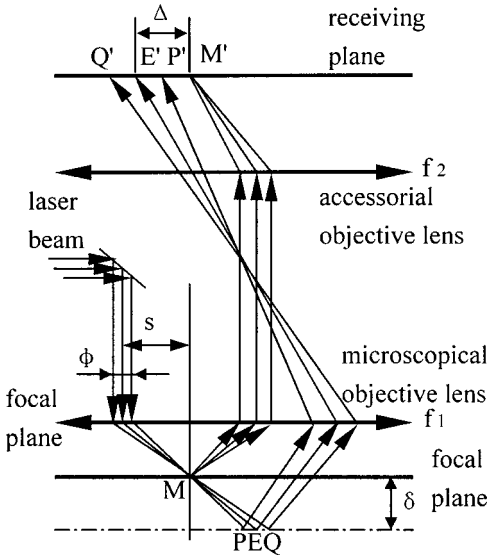

Fig. 2 Relationship between the sizes of the incident point and the image point.

2 Principle of the Eccentric Light Beam Method

2.1 *Relation between Defocus and the Movement of Light in the Image Plane*

The principle of eccentric light beam method is shown in Fig. 1. A laser beam, which is parallel to the primary optical axis with an offset *s*, is incident to the objective lens. And the object is imaged at point *M* in focus plane, then the reflected beam goes through the objective lens, as well as an accessory lens, and finally reaches point M' in the image plane. Points *M* and M' are conjugated points. When the measured plane defocuses an amount of $\pm\delta$, M' will generate a horizontal displacement $\pm\Delta$ in the ideal image plane. Supposing that the optical system is ideal, we can get the relation between δ and Δ according to the theory of geometrical optics:

$$tgu=\frac{s}{f_1}, \tag{1}$$

where *u* is the incident (reflect) angle; and f_1 is the focal length of the objective lens.

When the eccentric amount between the receiving plane (image plane) and the focal plane, called the defocused amount, is δ, the light point *M* moves to the point *N* in the focal plane; then, in the receiving plane (image plane), the displacement of the image point Δ will be

$$\Delta=\pm K_1\delta, \tag{2}$$

where δ is the defocused amount; K_1 is an optical constant, $K_1=(2\beta s)/f_1$; and β is the transverse magnification of the optical system, $\beta=f_2/f_1$.

As shown in Eq. (2), in the receiving plane, the displacement of the light point in the orthogonal direction of the optical axis is proportional to the defocused amount.

2.2 *Problem of Light Energy*

2.2.1 *Point size and photocell diameter in the receiving plane*

Equation (2) is deduced under an ideal light condition, however, the real light could not be an ideal straight line but beams with certain diameters. Also the diameter of the beam determines the size of the spot and its energy in the receiving plane. Thus, the diameter of the incident light and its energy will directly influence the sensitivity of the received signal.

Supposing that the diameter of the incident light is Φ, and the eccentric amount is *s* (as shown in Fig. 2), the spot diameter in the image plane will be

$$\phi'=2\phi\beta\frac{\delta}{f_1}=K_2\delta, \tag{3}$$

where $K_2=(2\phi\beta)/f_1$ is an optical constant. As shown in Eq. (3), we conclude that the spot size in the image plane is also proportional to the defocused amount.

In the receive plane, the diameter of the photocell *D* is

$$D\geqslant\frac{2\beta\delta}{f_1}(2s+\phi)=K_3\delta, \tag{4}$$

where $K_3=[2\beta(2s+\phi)]/f_1$ is an optical constant.

2.2.2 *Light intensity distribution*

Because the aperture of the microscope is limited, to avoid the light cutting in optical system, it is necessary to limit the size of the incident light beams. For a certain aperture, according to the theory of Fraunhofer diffraction at circular apertures,[10] the intensity in the image plane will be

$$I=I_0\left[\frac{2J_1(Z)}{Z}\right]^2 \tag{5}$$

where Bessel function $J_1(Z)$ is oscillatorily changed with a modification of Z.

Thus, the laser beam limited by the aperture will generate a circular symmetrical light distribution in the focal plane of the objective. Because we employ a specially designed aberration-free microscope system, after imaging through the microscopic system, the light distribution in the receiving plane is also circular symmetrical, ignoring the aberration of the microscopic system and the noise in the imaging process.

2.2.3 *Change of the energy center of the spot in the receiving plane with the modification of the defocused amount*

As shown in Eq. (3), the spot resulting from the laser beam in the receiving plane is in fact a light intensity distribution. When a position detector of the spot energy center is placed in the receiving plane, we must discuss the change of the spot energy center with the modification of the defocusing amount.

The defocused amount will cause

1. a change of the light intensity distribution. The defocusing will cause the loss of conjugate relationship between the reflecting plane and the receiving plane. The original light distribution in the receiving plane will be changed because of the defocusing.
2. the center of the light beam will generate the transverse displacement in orthogonal direction of the optical axis.

If it is in the focus, the center of the spot energy lies on the y axis (as shown in Fig. 3). The energy distribution on the two sides of y axis will be W_1, and W_2, respectively, where the energy distribution will be

$$W_1=\int_{-\infty}^{+\infty} \mathrm{d}y \int_{-\infty}^{0} I(x,y)\,\mathrm{d}x=\iint_{-} I(x,y)\,\mathrm{d}s, \tag{6}$$

$$W_2=\int_{-\infty}^{+\infty} \mathrm{d}y \int_{0}^{\infty} I(x,y)\,\mathrm{d}x=\iint_{+} I(x,y)\,\mathrm{d}s. \tag{7}$$

Suppose that the reflectivity of the reflection plane R is a constant. When defocusing, the spot in the receiving plane moves a displacement Δ (suppose that $\Delta<0$ when defocus is negative and $\Delta>0$ when defocus is positive). Thus, the spot energy distribution W_1 and W_2 will be changed to

$$W_1'=\int_{-\infty}^{+\infty} \mathrm{d}y \int_{0}^{\infty} I(x+\Delta,y)\,\mathrm{d}x, \tag{8}$$

$$W_2'=\int_{-\infty}^{+\infty} \mathrm{d}y \int_{0}^{\infty} I(x-\Delta,y)\,\mathrm{d}x. \tag{9}$$

Then the energy difference between two parts of the photocell is

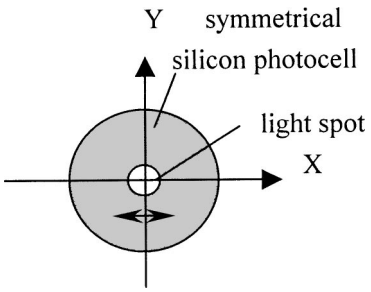

Fig. 3 Light energy distribution.

$$W=W_1'-W_2'=\int_{-\infty}^{\infty} \mathrm{d}y \int_{0}^{\infty} [I(x+\Delta,y)-I(x-\Delta,y)]\,\mathrm{d}x. \tag{10}$$

Note that $I(x,y)$ is an approximately Gaussian distribution of the light intensity:

$$I=(x,y)=\sqrt{2\beta}I_0 \exp[-2\pi\beta(x^2+y^2)]. \tag{11}$$

Then

$$\begin{aligned} W&=\sqrt{2\beta}I_0 \int_{0}^{\infty} \{\exp[-2\pi\beta(x+\Delta)^2] \\ &\quad -\exp[-2\pi\beta(x-\Delta)^2]\}\,\mathrm{d}x \\ &=2\sqrt{2\beta}I_0 \int_{\Delta}^{0} \exp(-2\pi\beta x^2)\,\mathrm{d}x. \end{aligned} \tag{12}$$

According to the integral mean value theorem

$$W=-2\sqrt{2\beta}I_0 \exp(-2\pi\beta\xi^2)\Delta \quad [\xi\in(0,\Delta)]. \tag{13}$$

When $\Delta\ll 1/(2\pi\beta)^{1/2}$, $\xi^2<\Delta^2\ll 1/2\pi\beta$, then $\exp(-2\pi\beta\xi^2)\approx 1$. From Eq. (2), we see that the relation between the defocusing amount and the energy difference of the two sides of y axis will be

$$W=K_4\delta, \tag{14}$$

where $K_4=-2\sqrt{2\beta}I_0$.

Actually, the sample is not an ideal single surface and includes coatings and surface steps at least, thus there will be multiple reflections from many surfaces and scatterances from surface steps. But these effects change only the spot energy on the receiving plane and do not change the spot shape, so the linear relation between W and δ shown in Eq. (14) will not be changed except for the change of constant K_4.

3 Design of the Autofocusing System

Figure 4 is a linewidth measuring system using the autofocusing principle represented here. The system consists of six parts: measuring light path, auto-focusing light path, monitoring system, sample and its work stage, control system, micro-scale compensation structure.

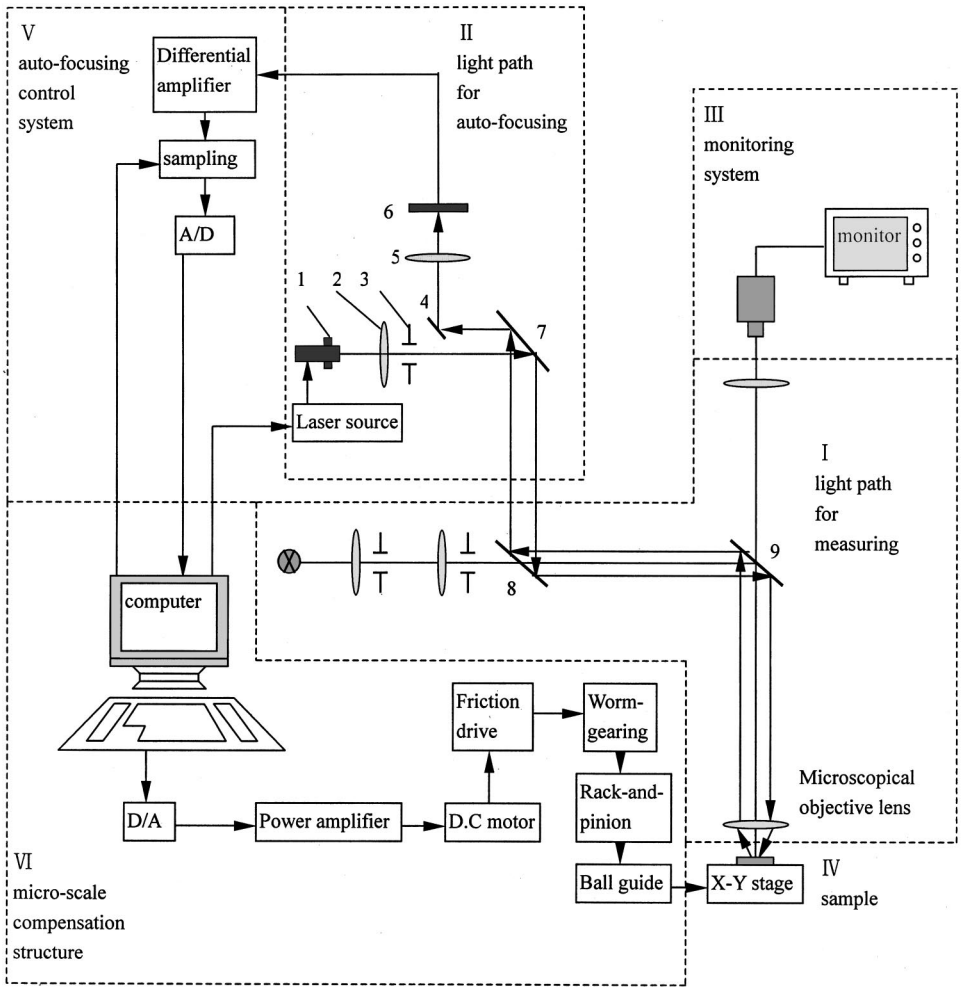

Fig. 4 Fundamental block diagram of the autofocusing system: A/D, analog to digital, and D/A, digital to analog.

3.1 *Autofocusing Light Path*

As shown in part II of Fig. 4, semiconductor laser 1 emits the laser beam ($\lambda=0.88\,\mu$m). The beam goes through a collimating objective (2), a diaphragm (3), a reflecting mirror (7), beamsplitters (8 and 9), and is incident on a micro-objective with an eccentric amount s, then forms the image of the measured sample, which is placed on the microscale platform. After reflecting, the beam goes back in the same way, diverting the incident light $2s$, through a reflecting mirror (4), an accessorial objective (5), then forms an image on the symmetrical silicon photocell 6 (Model 2CR61-2, Beijing Photo-electronic Device Factory, China, 1999) in the receiving plane. After the photoelectric conversion, an eccentric amount can be obtained.

The main problem in the design of the optoelectronic detector is how to obtain enough eccentric information without interfering with the microscope. This design employs an IR semiconductor laser device, which has some characteristics such as small size, large impulse power, high brightness, etc., and its wavelength is different from the working wavelength of the microscope. To solve the problem of light energy decrease, we employ a coated beamsplitter whose reflectivity is 100% for an IR wave and 50% for white light. The symmetrical silicon photocell serving

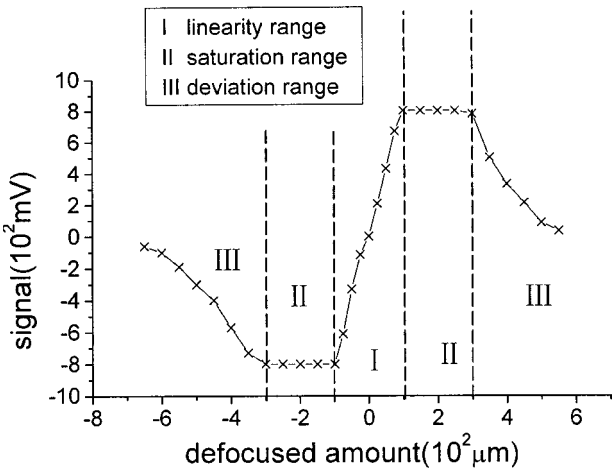

Fig. 5 Performance curve.

Table 1 Focusing precision of all kinds of the objectives.

Specification of the Objectives						Focusing Precision (μm)	
β	NA	WD (mm)	f (mm)	ε (mm)	Measured Plane	Up	Down
20×	0.4	3.0	11.6	0.8	Wafer reflection	0.08	0.04
40×	0.65	1.0	5.26	0.5	Mask transmission	0.10	0.09
50×	0.85	0.43	3.76	0.38	Wafer reflection	0.05	0.03
100×	0.9	0.23	2.13	0.37	Wafer reflection	0.09	0.06
100×	0.9	0.23	2.13	0.37	Mask transmission	0.08	0.05

Here β, magnification; NA, numeral aperture; WD, working distance; f, focal distance; ε, resolution; up indicates the focusing precision when stage goes upward; and down when it goes downward.

as the receiver has high sensitivity, whose spectral response peak wave is about $\lambda=0.8\,\mu$m, which matches the spectrum of the semiconductor laser. After differential amplification of the defocused signals, we can decide whether the eccentric amount is positive or negative, and an ideal defocused signal is then obtained.

3.2 *Autofocusing Control System*

A block diagram of control system is also shown in part V of Fig. 4. After a differential amplification, the eccentric signal is sampled, converted through an A/D converter, and is received by the receiver into a microprocessor. The output signal, after D/A the converter and power amplification, drives a dc motor to move a microstructure to compensate the eccentric amount.

3.3 *Microsacle Compensation Structure*

The compensation microstructure is the actuator to fulfill the autofocus, whose precision and mobility directly influences the precision of the autofocus. This design employs a microscale mechanic structure, whose block diagram is shown in part VI of Fig. 4. The voltage output of the control system drives the dc motor through the friction drive, worm-gearing, rack-and-pinion, and ball guide and then moves the working platform to compensate errors.

4 Experimental Results and Analysis

After the system was completed, tests were conducted using five objectives made in China with different magnifications. We also employ a TESA inductance micrometer dial with a resolution of $0.01\,\mu$m and a 2‰ nonlinearity. The test results are shown as follows.

4.1 *Focusing Range*

The test result for the focusing range is shown in Fig. 5. The curve can be divided into three segments: the linearity range, the saturation range, and the deviation range. When the defocusing range is within $\pm 100\,\mu$m, the linearity is good, and the sensitivity is the highest. Within 100 to $300\,\mu$m and -100 to $-300\,\mu$m is the saturation range, which begins when the whole spot enters one quadrant of the symmetrical silicon photocell and ends when the whole spot begins to leave the silicon photocell. In this range, as the silicon photocell receives the light, the output signal of the spot movement is almost invariant; that is, the additional output caused by the defocused amount is invariant. Within the range >300 and $<-300\,\mu$m, with the addition of the defocused amount, the spot tends to leave the silicon photocell and the signal becomes smaller and smaller. Finally, all the spots leave the silicon photocell and the signal returns to zero, which means it is out of the defocusing range. Because of using the differential amplifier, a positive or negative defocused signal exists in the saturation range and in the deviation range. This signal drives the motor to rotate positively (or negatively), compensating the defocusing amount, and causing it to enter the linearity range, then slowing down and fine focusing. Thus, the focusing range will be $\pm 500\,\mu$m.

4.2 *Focusing Precision*

For the objectives mentioned, we tested the autofocusing precision when positively or negatively defocusing in reflective illumination or transparent illumination, separately. We tested 20 times in every condition. Calculating all the data with Eq. (15), we can acquire the focusing precision of all kinds of objectives (see Table 1).

$$\sigma=\pm\left[\frac{\Sigma(x_1-\overline{x})^2}{N-1}\right]^{1/2} \tag{15}$$

5 Conclusion

The eccentric light beam method proves to be an autofocusing method with high resolution, as well as a large focusing range. The device has a compact structure. The theoretical formula of the eccentric light beam method can be applied not only to an object lens whose objective plane is just the focal plane, but also to an object lens whose objective plane is not the focal plane. The experimental results indicate that the focusing range is up to $1000\,\mu$m, while the focusing precision can reach $\pm 0.1\,\mu$m. The system has high reliability and can meet the requirements of various accurate micromeasurement systems.

Acknowledgments

This project was supported by the Tsinghua University Research Foundation project 985. The authors wish to acknowledge Xianhai Xu and Lianqing Zhang for their constructive work on the experiments. Thanks also go to Prof. Boxiong Wang who gave us many helpful suggestions.

References

1. S. Xue and Q. Li, *Design of Precision Instruments*, pp. 230–240, Tsinghua University Press, Beijing, China (1990) (in Chinese).

2. G. Bouwhuis and J. J. M. Braat, ''Video disk play optics,'' *Appl. Opt.* **17**(13), 1993–1999 (1978).
3. D. K. Cohen, W. H. Gee, M. Ludeke, and J. Lewkowicz, ''Automatic focus control: the astigmatic lens approach,'' *Appl. Opt.* **23**(4), 565–570 (1984).
4. C. Bricot, J. C. Lehureau, and C. Peuch, ''Optical readout of videodisc,'' *IEEE Trans. Consum. Electron.* Nov. (1976).
5. H.-P. Ho, S. Y. Wu, K.-S. Chan, E. Y. B. Pun, and P. Shum, ''Multilayered optical disc scheme for high density storage using transparent media,'' *Jpn. J. Appl. Phys., Part 2* **39**(6), L597–L600 (2000).
6. P. L'Hostis, F. Byers, F. Podio, and X. Tang, ''Microscopic image analysis of defect areas in optical disks,'' *Proc. SPIE* **3806**, 106–112 (1999).
7. C. N. Cho, S. K. Kang, J. S. Yoon, and J. K. Paik, ''Digitial autofocusing of multiple object based on image restortation,'' *Proc. SPIE* **4067**, 1642–1651 (2000).
8. S. Hong, J. Hwang, and B. Nam, ''Motion detection of the low-cost surveillance camera system,'' *Proc. SPIE* **3965**, 269–276 (2000).
9. G. Udupa, M. Singaperumal, R. S. Sirohi, and M. P. Kothiyal, ''Characterization of surface topography by confocal microscopy: I. Principles and the measurement system,'' *Meas. Sci. Technol.* **11**(3), 305–314 (2000).
10. Q. Liang, *Physical Optics*, pp. 122–125, Mechanical Industry Press, Beijing, China (1983) (in Chinese).

Qingxiang Li graduated in 1965 from Tsinghua University where he became a professor and doctor mentor in 1994. He directs the Precision Machinery Society and is a member of the Teaching Guide Committee for Electromechanical of Colleges and Universities over the whole country. His current research interests include precision instruments and micromechanics. He has published 10 books, authored 100 journal papers, and applied for five patents.

Lifen Bai received her BS and MS degrees in precision instruments from Tsinghua University, Beijing, China, in 1991 and 1994, respectively, where she is currently a lecturer. Her research interests include precision measuring, image processing, microsensors, and actuators.

Shifu Xue graduated in 1954 from Dalian Institute of Technology and received his MS degree in 1956 from Tsinghua University, where he became a professor in 1990. He has worked in the areas of precision instruments, semiconductor manufacture, and measurement equipment and has authored 70 journal papers.

Luyun Chen graduated in 1999 from Tsinghua University, where she is currently engaged in her MS program with Prof. Li. Her main research interests are precision instruments, control, and microelectromechanical systems.